Stratifying Forest Overstory and Understory for 3-D Segmentation Using Terrestrial Laser Scanning Data

Zengxin Yun and Guang Zheng

***Abstract*—Accurately and rapidly segmenting tree crowns from a three-dimensional (3-D) perspective is of great significance to precision forest management, and better understands the carbon and water cycles between the soil–plant–atmosphere system. However, it remains challenging to group points into individual trees from a 3-D perspective in the forest stand with highly overlapped tree crowns and abundant understory. The objective of this article was to extract the overstory and understory of individual trees from terrestrial laser scanning (TLS) data considering the vertical forest structure and overlapped tree crowns processing strategy suitable for various crown shapes and sizes. Our results showed that 1) the proposed algorithm had better performance in the low overlapping rate (OR) coniferous (F1-score: 0.96) and broadleaf (F1-score: 0.91) forest stands, while the F1-score decreased down to 0.89 and 0.65 in the high OR for coniferous and broadleaf forest stand, respectively; 2) a multistation TLS data produced better (F1-scores: 0.85–1) segmentation results than those obtained from single-station TLS data (F1-scores: 0.67–0.83) in coniferous forest stands; and 3) the vertical forest structure profiles affected the final forest 3-D segmentation accuracy. Our article provides a solid foundation for precision forestry and natural resources management.**

***Index Terms*—Forest segmentation, forest structure, terrestrial laser scanning (TLS).**

I. Introduction

FOREST ecosystem, accounting for 30% of the global non-ice covered land, is one of the most important terrestrial ecosystems on the earth and plays a crucial role in the carbon and water cycles of soil–plant–atmosphere biospheres [1], [2]. Forest inventory is the basis and prerequisite for monitoring forest resource dynamic changes accurately and efficiently [3], [4]. Separating individual tree crowns has become a prerequisite for estimating forest structural parameters, including tree height [5], diameter at breast height (DBH) [6], crown volume [7], and biomass estimation [8]. These parameters are essential inputs to some process-based forest carbon and water cycle simulation models [9], [10].

Manuscript received May 24, 2021; revised August 6, 2021 and October 12, 2021; accepted November 11, 2021. Date of publication November 23, 2021; date of current version December 8, 2021. This work was supported in part by the National Science Foundation of China under Grant 41771374, and in part by the Key Research and Development Programs for Global Change and Adaptation under Grant 2019YFA0606601. *(Corresponding author: Guang Zheng.)*

Zengxin Yun is with the International Institute for Earth System Science, Nanjing University, Nanjing 210023, China, and also with the Jiangsu Provincial Key Laboratory of Geographic Information Science, Nanjing 210023, China (e-mail: yzx_nju@163.com).

Guang Zheng is with the International Institute for Earth System Science, Nanjing University, Nanjing 210023, China (e-mail: zhengguang@nju.edu.cn).

Digital Object Identifier 10.1109/JSTARS.2021.3129312

Overall, traditional methods to delineate tree crowns included field-based methods and remotely sensed data-based methods. The most common field-based method is to record the number and locations of trees manually in the forest. However, the time-consuming and labor-intensive nature and personal subjective factors of the field-based inventory measurements limit their application in the broader spatial scales with high accuracy [11]–[13]. There are two different kinds of methods based on the types of remotely sensed data: 1) Raster imagery-based methods: some studies have delineated tree crowns based on the two dimensional (2-D) images by applying existing digital image processing techniques [14], [15], for example, those methods based on edge detection [16], region growing [17], and watershed segmentation [18]. However, they fail to capture the vertical profile of the 3-D forest structure, which is essential to characterize forest structural parameters [10], [19]. Moreover, the image interpolation processing procedures introduce errors to the forest structural parameters estimation [20]. 2) Point data-based method: the advance of the light detection and ranging (lidar) technology allows mapping forest structure from a 3-D perspective in a nondestructive manner [21], [22]. Aerial laser scanning (ALS), terrestrial laser scanning (TLS), and mobile laser scanning (MLS) are the most commonly used platforms in the domain of small-footprint lidar systems [23], [24]. TLS and MLS capture detailed 3-D structures of understory and lower canopy components with high spatial resolution at millimeter level, and while ALS records more upper components of forest with relatively low-density point cloud data at point spacing of decimeter level [25]–[27]. Some crown delineation algorithms had been developed for ALS data successfully [21], [28]–[30]. However, the inherent differences from ALS's system and data characteristics require specific algorithms developed for TLS and MLS data [8], [23]. Tree crowns segmentation based on TLS and MLS data can be used to model tree stems, DBH estimation, and characterize overstory and understory distribution with high accuracy [31]–[34]. Some researchers have attempted to segment tree crowns based on the voxel data structure. For example, Xi *et al.* [35] adapted an anchor-free deep learning model, CenterNet, to detect individual tree crowns from TLS data. But the smaller or larger trees with overlapped areas could not be detected effectively due to the limited samples. In addition, they ignored the effect of understory on segmentation. Luo *et al.* [36] proposed an approach based on the deep pointwise direction to extract individual trees from MLS data. However, there were still some separation errors at the boundaries of the instance-level trees especially the overlapped areas. However,

TLS can be placed in the high-density forest with overlapped regions where vehicles cannot reach, but MLS was mainly used to obtain roadside trees information [37]. Others grouped points into individual trees with identified tree stem locations directly based on the point information without converting points into voxel structure. For example, Tao *et al.* [8] used a density-based spatial clustering of applications with noise (DBSCAN) algorithm to identify trunks, and then segmented the crowns according to the distance of points to the trunk based on the Dijkstra's shortest path algorithm [38]. Cabo *et al.* [39] approximated the individual tree crown boundaries with the Voronoi diagram [40], but they failed to define the real boundaries of tree crowns accurately. However, it remains challenging to segment tree crowns using TLS data due to the complexity of vertical forest structure (overstory–understory) [41]–[43], species differences [44]–[46], and understory abundance [42]. Few studies have considered the existence of understory when extracting trees based on TLS data. The occlusion of the understory will affect tree stem identification, crown segmentation, tree height, and crown width estimation [8], [42], [43], [47], [48]. The heavily overlapped tree crowns with varied sizes further challenge the tree crowns segmentation. Hyyppa *et al.* [49] and Popescu *et al.* [50] noticed that ignoring the overlapping problem would underestimate tree crown size and volume. Tao [51] realized that accurate segmentation of overlapped tree crowns affected forest aboveground biomass and crown volume estimation accuracy. It is still an unsolved question about better segmenting tree crowns, especially in the overlapped areas from a 3-D perspective. Therefore, in this article, we proposed a method to extract the individual overstory and understory considering the effect of understory and overlapped tree crowns. The overall goal of this article is to segment forest from TLS data, and the specific goals are to: 1) develop an algorithm to segment forest trees using TLS data; and 2) investigate the effects of overlapping rate (OR), the number of TLS scanning stations, forest types, vertical forest structure, and point density on the accuracy of 3-D tree crowns segmentation. Flowchart of tree crowns segmentation was at Fig. 1. The whole process of trees segmentation can be divided into two modules. The first is tree trunk identification (searching sphere technique) after the forest stratification processing (overstory and understory). The second is to refine the segmentation result using multiple planes segmentation technique based on the result of coarse segmentation (spacing-based clustering).

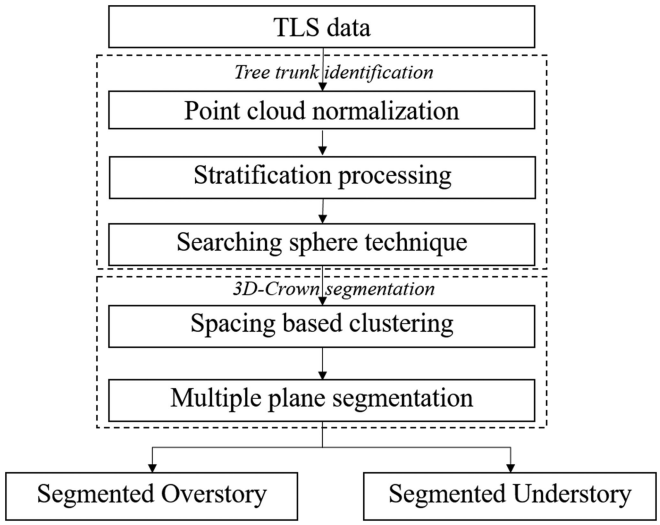

Fig. 1. Flowchart of 3-D tree crown segmentation.

II. Materials

A. Study Sites

There are two different sites with homogeneous and heterogeneous forest in southern Finland and the Pacific Northwest.

The first study site was located in the Evo natural homogeneous forest (61.19°N, 25.11°E) with dominant tree species of Scots pine (*Pinus sylvestris L.*), Norway spruce (*Picea abies L. Karst*), silver birch (*Betula pendula Roth*), and downy birch (*Betula pubescens Ehrh.*) [Fig. 2(a)]. The average DBH in the Evo forest varied from 10 to 35 cm with understory. We selected six different forest plots with 32 m × 32 m with varying numbers of trees. The average overstory and understory height at six plots were 9.52–22.77 m and 2.11–6.63 m, respectively (Table I).

The second study site was the Washington Park Arboretum (WPA) (122°17′46″ W, 47°38′08″ N), a well-managed urban heterogeneous forest [Fig. 2(b)] located south of the University of Washington campus in Seattle, WA, USA There are more than 4600 species with a maximum tree height of 64.7 m. The dominant tree species at the WPA were Douglas fir (*Pseudotsuga menziesii*), Western hemlock (*Tsuga heterophylla*), Western red cedar (*Thuja plicata*), Big-leaf maple (*Acer macrophyllum*), Monkey puzzle (*Araucaria araucana*), Southern magnolia (*Magnolia grandiflora*), and New Mexican locust (*Robinia neomexicana*). We set up three circular plots with radii of 30 m in the WPA site. The average overstory and understory height at three plots were 16.28–30.93 m and 5.96–6.75 m, respectively (Table I).

B. Datasets

1) Terrestrial Laser Scanning Data: The Evo data is the open data from the EuroSDR TLS international Benchmarking project [52]. The TLS data were collected in April and May 2014, using the Leica HDS6100 with a laser wavelength of 650–690 nm and a field of view of 360° (horizontal) × 310° (vertical). The distance measurement accuracy was ±2 mm at 25 m away from the scanner. The angle increment was 0.036° in both horizontal and vertical directions, which resulted in a point spacing of 15.7 mm at 25 m away from TLS (Table II). TLS collected data at the center point first, and four additional corner points in each squared forest plot with a 5-min long TLS scanning in each location. Six artificial spheres with a radius of 198 mm were used as reference targets for data registration in each plot. All five scans in each plot were registered using targets and merged as multiscan TLS data with an average registration accuracy of 2.1 mm.

In the WPA site, the TLS data were collected using the Leica Scan Station 2 system with a laser wavelength of 532 nm. Among

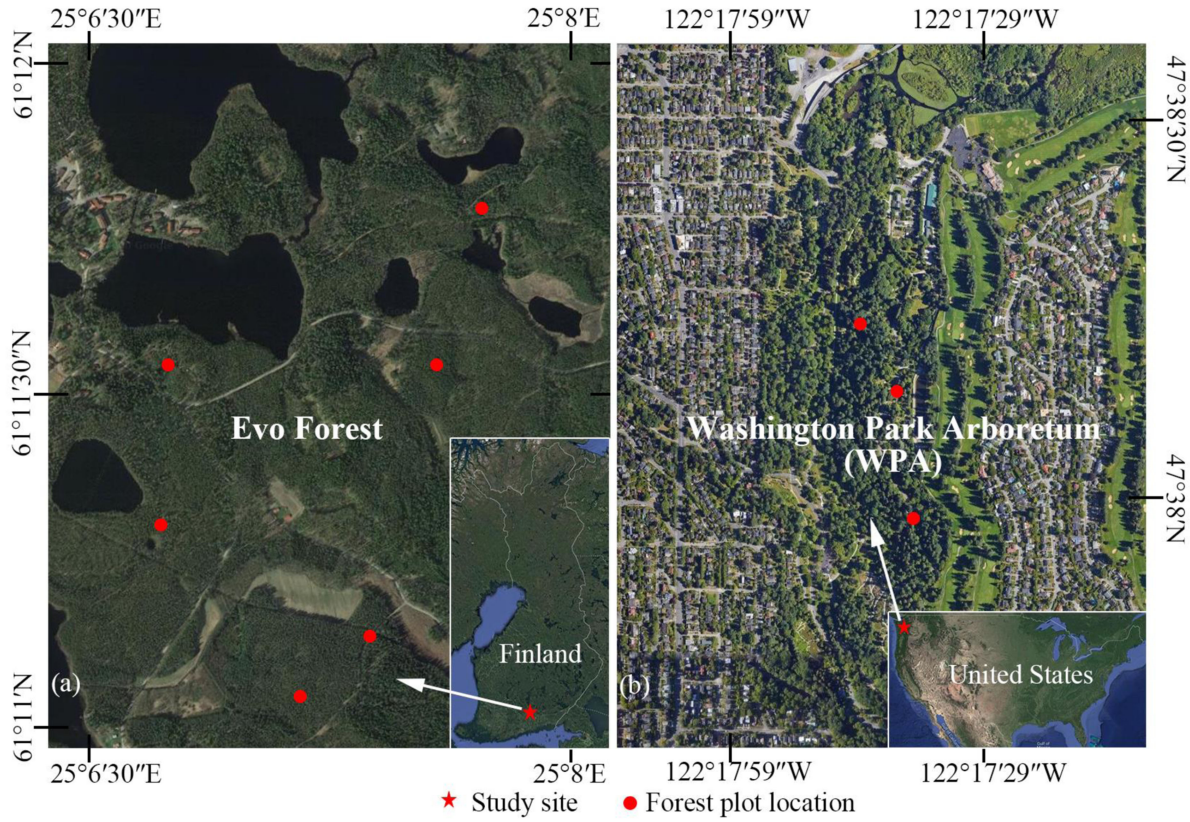

Fig. 2. Study sites used in our article. (a) Study site 1: Evo forest in Finland. (b) Study site 2: WPA forest, in Washington State, USA.

TABLE I
PLOTS INFORMATION OF EVO FOREST AND WPA FOREST

Plots	Density	Number of trees	OR	Average overstory height (m)	Number of understory	Average understory height (m)
Evo-LC1	low	27	4.3%	22.77	19	4.74
Evo-LC 2	low	36	13.8%	21.31	9	6.63
Evo-LC 3	low	43	12.4%	18.05	23	2.35
Evo-HC 4	high	55	35.8%	21.67	20	3.31
Evo-HC 5	high	92	45.1%	16.06	32	3.82
Evo-HC 6	high	145	51.2%	9.52	18	2.11
WPA-LB1	low	6	6.5%	16.28	7	5.99
WPA-LM2	low	8	26.4%	30.93	6	6.75
WPA-HB3	high	17	54.2%	22.43	0	0

OR represents the overlapping rates of tree crowns. Evo-LC1, Evo-LC2, and Evo-LC3 are the low-density coniferous plots in the Evo forest. Evo-HC4, Evo-HC5, and Evo-HC6 are the high-density coniferous plots in the Evo forest. WPA-LB1 is the low-density broadleaf plot at WPA. WPA-LM2 is the low-density mixed tree species plot at WPA. WPA-HB3 is the high-density broadleaf plot at WPA.

each forest plot, the TLS scanner was set up at the center position with a whole field of view (i.e., horizontal: 0°–360° and a vertical scan angle of −45°–90°). The minimum angle resolution was 0.3 mm (3e-06 radians) with a scanning speed of 50 000 pts/s. The laser sampling spacing was set at 0.1 m at 30 m (Table II).

2) Validation Data: To validate the computer-based tree crowns segmentation, we visually identified the tree stem locations, heights, and total tree number for both overstory and understory based on TLS data in two study sites (Table I). To ensure accuracy, we used order from plot edge to center for measuring the trees in the 3-D software (CloudCompare). For example, we manually measured the trees located at the plot edge without occlusion, and carefully cut out these trees measured. We repeated this process in the rest point cloud to measure all the trees in the center of the plot. For trunk position, three people recorded the coordinates of overstory trunks at 1.3 m, and the coordinates of understory trunks at 0.5 m from three different directions. Three people measured the distances from treetop to the ground points identified manually to evaluate the obtained tree height. The mean values of trunk positions

TABLE II
PARAMETERS OF TERRESTRIAL LASER SCANNER

Leica HDS6100	Wavelength of continuous wave	0-690 nm
	Field of view	360°×310°
	Distance measure accuracy	±2 mm at 25 m
	Angle increment	0.036°
	Data collection mode	High density
	Point spacing	15.7 mm at 25 m
Leica Scan Station 2	Wavelength	532 nm (visible green light)
	Field of view	360°×270°
	Minimum angle resolution	0.3 mm (3d-06 radians)
	Scanning speed	50,000 pts/sec

and distances were viewed as the actual values. Three people manually measured the tree crowns' width in the North–South and West–East directions. We took the average crown width as the final result, and calculated the OR between the nearest trees. Section III-C described the detailed calculation method of the OR. The average OR at the plot was set as the OR of a forest plot. We divided all the forest plots with varying overlapped tree crowns into two groups: low-density (low OR, OR $< 27.1\%$) and high-density (high OR, OR $> 27.1\%$, which was half of the OR maximum value at all the plots) (Table I).

III. METHODS

A. Tree Trunk Identification

Tree trunk identification was the first step of trees segmentation, including seed points identification and trunks tracing.

1) Seed Points Identification: To avoid the effects of forest understory on identifying tree trunk seed points, we first stratified overstory and understory layers based on the predefined height threshold. We filtered the ground points using the cloth simulation filter (CSF) algorithm [53], then the lowest point method was used to extract more accurate ground points from the CSF filtering result [54]. A digital terrain model (DTM) with a resolution of 0.5 m was generated through interpolating ground points using the ordinary Kriging method provided by the ArcGIS software. We then obtained the height-normalized points by subtracting the corresponding terrain elevation from the DTM model and vegetation points by removing all ground points. A sixth-order polynomial curve function was fitted to the vertical profile of point density in each height bin with a fixed interval to determine the stratification surface. The sixth-order polynomial curve function used was

$$y = B + \sum_{i=1}^{6} A_i x^i. \tag{1}$$

B is the intercept of the polynomial. A_i ($i = 1 \ldots 6$) is the corresponding coefficient of x^i, and their values are determined by the least square method. We obtained the initial dividing height (H_0) where the first-order derivation was zero, and the second-order derivation was larger than zero [Fig. 3(a)] [42], [55], [56]. If multiple values of H_0 were detected, the ones would be invalid if they were near to treetop. The stratification surface could be produced by adding the DTM with the height threshold H_0 [Fig. 3(a)]. Then, we extracted the points from the bin with heights ranging from H_0 to $H_0 + 0.2$ m to detect tree trunks of the overstory by assuming the tree trunks were cylindrical geometric objects. The cylindrical geometric object in 3-D space was approximated as (2):

$$\begin{aligned}&(x - x_{i0})^2 + (y - y_{i0})^2 + (z - z_{i0})^2 - r^2 \\ &\quad = \frac{\left[l_{\{i}\,(x - x_{i0}) + m_i\,(y - y_{i0}) + n_i\,(z - z_{i0})\right]^2}{\left({l_i}^2 + {m_i}^2 + {n_i}^2\right)}\end{aligned} \tag{2}$$

where $p_{i0}(x_{i0}, y_{i0}, z_{i0})$ ($i = 1, 2, \ldots, Q$) is the ith geometric center point of the cylinder with the axis $\overrightarrow{\boldsymbol{L}}_i(l_i, m_i, n_i)$; Q is the total number of tree trunks detected in the height bin ranging from H_0 to $H_0 + 0.2$ m; and r is the cross-sectional radius of the cylinder. We detected the cylindrical tree trunks within the extracted height bin using the RANdom SAmple Consensus (RANSAC) algorithm [57] with the total least square method. By doing this, we obtained the unknown parameters of the cylindrical mathematical model [Fig. 3(b)]. Then, we labeled the points constituting a cylinder as tree trunk points and used the point $\boldsymbol{p}_{i0}(x_{i0}, y_{i0}, z_{i0})$ as the first seed point for each tree trunk. The model distance threshold (MDT) is defined as the maximum distance between a given point and geometric cylinder model. It is critical for controlling the final extracted results in the RANSAC algorithm.

2) Trunk Tracing: To obtain the trunk points, starting from the first seed point $\boldsymbol{p}_{i0}(x_{i0}, y_{i0}, z_{i0})$ as the center point, two searching spheres with the radii of R_1 and R_2 ($R_2 > R_1$ and $R_2 > r$) were applied to each tree to identify tree trunk points in both upward and downward directions [Fig. 3(c)]. R_1 was defined as the radius of the inner searching sphere used in the trunk point identification. The tree trunk diameter within this horizontal slice was a good reference for the value of R_2. The value of R_2 would determine the thickness of the horizontal slice and further the level of details of tree trunk curvature.

As for the upward direction, we computed the geometric center point $\boldsymbol{p}_{i1}(x_{i1}, y_{i1}, z_{i1})$ for all the points within the horizontal slice whose heights ranging from $z_{i0} + R_1$ to $z_{i0} + R_2$ (*a new sphere center could replace* $\boldsymbol{p}_{i0}$ *at the next step*). Then the vector $\overrightarrow{\boldsymbol{p}_{i0}\boldsymbol{p}_{i1}}$ was the growing direction of the tree trunk in local 3-D space. The point $\boldsymbol{p}_{i1}(x_{i1}, y_{i1}, z_{i1})$ would be the new center of the

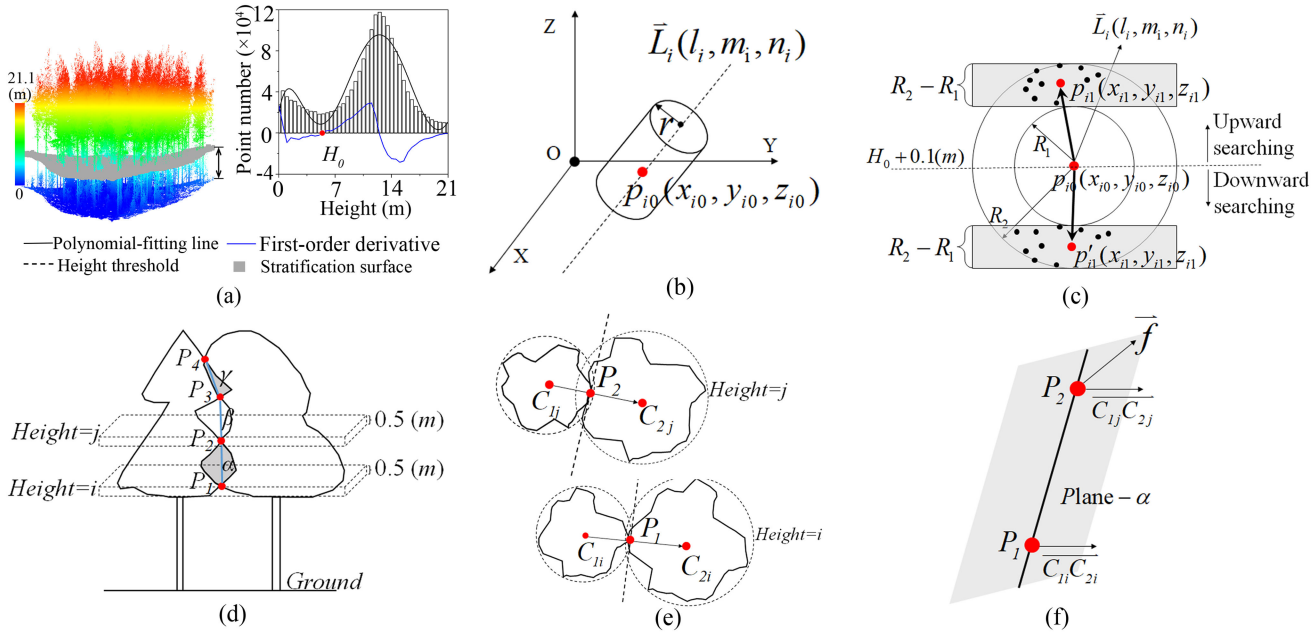

Fig. 3. Schematic diagram of tree segmentation. (a) H_0 determined using statistics method. (b) Trunk seed point identification. (c) Trunk points identification. (d) Schematic diagram of the crown segmentation process. (e) Changing points determination at Height $= i$ and Height $= j$. (f) Segmentation plane—α determined by calculation.

two searching spheres to identify tree trunk points consecutively. Meanwhile, we also computed the maximum distance $D_{i1\_\max}$ between the points within a horizontal slice and geometric center. The iterative process would stop if the maximum distance within a horizontal slice was larger than the reference threshold, larger than the value of r. Usually, the upward searching process stops at the crown base height. The same searching spheres algorithm was also applied to the downward direction with the starting seed point $\boldsymbol{p}_{i0}(x_{i0}, y_{i0}, z_{i0})$. By computing the geometric center point $\boldsymbol{p'}_{i1}(x_{i1}, y_{i1}, z_{i1})$ for all the points within the horizontal slice whose heights ranging from z_{i0}–R_2 to z_{i0}–R_1, the iterative process would continue until reaching the ground surface. Finally, we identified and extracted tree trunk points from the ground surface to crown base height at plot level and stored them separately.

B. Forest 3-D Crown Segmentation

After extracting all tree trunks points, we then segmented tree crowns for both overstory and understory by following two steps:

1) Initial Segmentation: For each identified tree trunk point set, we first sorted the rest of the points in the forest plot in the height-increasing order. We computed the minimum 2-D distances ($d_{\min-1}$) between a to-be-classified point and the identified tree point set (I). The point would not belong to the tree if the $d_{\min-1}$ was larger than the threshold D_t. It would be moved to the classified point set (U). The determination of Dt could refer to the effect of spacing threshold in research [28]. For the point whose $d_{\min-1}$ values were smaller than the threshold D_t, we computed the 3-D minimum distance between the point and the point sets-I ($d_{\min-2}$) and U ($d_{\min-3}$). The point would belong to the point set that had a smaller distance. For example, if the $d_{\min-2} < d_{\min-3}$, the point would be allocated to the point set-I. We would repeat the above process for all of the rest to-be-classified points iteratively until they were all labeled. Based on the identified tree trunk point sets at the forest plot level, we could group all individual tree points to obtain the preliminary segmentation results.

2) Overlapped Area Division: For the overlapped areas of the preliminary segmentation results of the trees, we first conducted the horizontal point cloud slicing with a height interval of larger than neighbor point distance (NPD) [58] (for example, 0.3–0.5 m). We detected the number of point clusters for each horizontal slice using the DBSCAN algorithm [59]. The neighbor radius is a crucial parameter of the DBSCAN algorithm. Multiple overlapped areas could be identified within a single slice bin.

Based on the DBSCAN algorithm, we were able to identify the changing point where the number of multiple point clusters merged into one. Therefore, we needed to apply the DBSCAN algorithm in two vertical directions (i.e., from bottom to treetop and from treetop to bottom) to identify all possible changing points of the number of point clusters in overlapped areas. Then, we connected the two neighbor changing points to construct a new vector, and further produced a segmentation plane combining the vector determined by the two geometric center points of two-point clusters [Fig. 3(d)], for example, for given two individual trees with overlapped areas. In the bottom to treetop direction, for the horizontal slice bin at the Height $= i$, the bottom of the overlapped areas [Fig. 3(e)], the two-point clusters produced by the DBSCAN algorithm could produce a new vector $\overrightarrow{\boldsymbol{C_{1i}C_{2i}}}$ using their geometric centers $\boldsymbol{C_{1i}}$ and $\boldsymbol{C_{2i}}$. We could detect the boundary point ($\boldsymbol{P_1}$) by connecting the two geometric center points of two-point clusters in this vector direction. The

number of point clusters produced by the DBSCAN algorithm changed from two to one at this height. By doing this, we could detect the changing points $\boldsymbol{P_1}$ and $\boldsymbol{P_3}$ [Fig. 3(e)] by slicing tree crowns iteratively from bottom to treetop. We could identify the changing points $\boldsymbol{P_2}$ and $\boldsymbol{P_4}$ when going through the horizontal slice bins from the treetop to the bottom using the DBSCAN algorithm. A new vector $\overrightarrow{\boldsymbol{f}}$ can be obtained based on $\boldsymbol{P}_1\boldsymbol{P}_2$ and $\overrightarrow{\boldsymbol{C}_{1\boldsymbol{j}}\boldsymbol{C}_{2\boldsymbol{j}}}$. The segmentation plane was constructed based on the normal vector $\overrightarrow{\boldsymbol{n}}$ and a point on the segmentation plane [Fig. 3(f)]:

$$\overrightarrow{\boldsymbol{f}} = \overrightarrow{\boldsymbol{P}_1\boldsymbol{P}_2} \times \overrightarrow{\boldsymbol{C}_{1\boldsymbol{j}}\boldsymbol{C}_{2\boldsymbol{j}}} \tag{3}$$

$$\overrightarrow{\boldsymbol{n}} = \overrightarrow{\boldsymbol{f}} \times \overrightarrow{\boldsymbol{P}_1\boldsymbol{P}_2} \tag{4}$$

$$A(x - x_0) + B(y - y_0) + C(z - z_0) = 0 \tag{5}$$

where *(A, B, C)* is the normal vector $\overrightarrow{\boldsymbol{n}}$. *($x_0$, y_0, z_0)* is the coordinate of point P_1. *(x, y, z)* is the coordinate of a point on the plane-α ($\overrightarrow{\boldsymbol{P}_1\boldsymbol{P}_2}$). Coordinate values in point cloud were taken into (5) iteratively and compared equation result with 0. Points satisfied equation result > 0 and equation result < 0 were on the plane's different sides, and points satisfied equation result $= 0$ were on the plane. Crown intersection parts in the forest can be separated from each other in this way. Trees segmentation schematic can be seen in Fig. 3.

Moreover, we could also obtain the consecutive segmentation plane-β ($\overrightarrow{\boldsymbol{P}_3\boldsymbol{P}_2}$) and plane-$\gamma$ ($\overrightarrow{\boldsymbol{P}_4\boldsymbol{P}_3}$). Based on all three segmentation planes, we could effectively divide the overlapped regions between two trees. In the case of multiple overlapped tree crowns, we would follow the procedures designed for two tree crowns described in Sections III-B.1 and III-B.2 at a time. After processing all possible combinations of the multiple tree crowns and grouping the points belonging to the same tree crown, we would achieve the final crown segmentation results for the trees.

For the understory points, a horizontal slice bin would be set up at the height (30% of the maximum height) to detect the seed point for each understory crown using the DBSCAN algorithm. Each clustering obtained was considered as an understory seed point. Once all seed points were found, we would follow the similar segmentation procedures described in Section III-B to allocate points of the forest understory.

3) Accuracy Assessment: To evaluate the accuracy of 3-D forest crown segmentation, we computed the recall (r), precision (p), and F1-score parameters as follows (6), (7), (8):

$$r = \frac{TP}{TP + FN} \tag{6}$$

$$p = \frac{TP}{TP + FP} \tag{7}$$

$$F1 = 2 \times \frac{r \times p}{r + p} \tag{8}$$

where TP is the number of correctly extracted tree locations; FN is the number of falsely extracted tree locations; FP is the number of falsely extracted nonexisting tree locations; *r* represents the completeness of crown segmentation; *p* describes the correctness of crown segmentation; and F1-score is the overall accuracy considering both commission and omission.

C. Sensitivity Analysis

MDT and R_2 are the key parameters affecting seed points and trunk points identification. By applying different MDT values ranging from 0 to 0.03 m with a step of 0.002 m, we investigated the effects of MDT on seed point identification for forest stands with and without understory. Moreover, we changed searching radii ranging from 0 to 1.5 m with a step of 0.05 m to test the effects of searching radius R_2 on forest types. The individual coniferous and broadleaf trees' heights were 21.8 and 25.1 m, and the crown widths were 5.3 and 20.2 m, respectively.

We changed the values of the neighbor radius from 0 to 1 m with a step of 0.03 m to explore their effects on identifying changing points using the DBSCAN algorithm. Three different groups (coniferous, broadleaf, and coniferous + broadleaf) with varied ORs and different tree species were used as test data. Then, we calculated a parameter named "changing point offset," defined as the offset distance between the actual changing points identified by visual inspection and the changing points produced from a computer-based algorithm:

$$\text{Offset} = \sqrt{\left(\Delta D_1^2 + \Delta D_2^2 + \ldots\ldots + \Delta D_i^2 + \ldots\ldots + \Delta D_n^2\right)/n} \tag{9}$$

where $\Delta {D_i}^2$ represents the 3-D Euclidean distance between the *i*th visual-based changing point and computer-based changing point, and *n* is the total number of the changing points.

We conducted overlapping experiments using three groups with different tree species to investigate the effects of OR. The sum of half the crown width of two trees was denoted by *q*. Distance between two trees at different overlapping degrees was calculated and denoted by *q'*, then we used *q'* and *q* to describe the overlapping degree of two trees:

$$\text{OR} = 1 - \frac{q'}{q} \tag{10}$$

where OR is a variable that defined the overlapping degree of two trees: 1) we conducted the overlapping experiments based on two coniferous trees (height: 21.8 m and crown width: 5.3 m) with the distance from 5 m (OR $= 0$) to 1.25 m (OR $= 0.75$) with a step of 0.625 m (OR $= 0.125$); 2) we used two broadleaf trees (height: 25.1 m and width: 20.2 m) using distance from 20 m (OR $= 0$) to 5 m (OR $= 0.75$) with a step of 2.5 m (OR $=$ 0.125); and 3) a broadleaf tree (height: 25.1 m and crown width: 20.2 m) and a coniferous tree (height: 24.3 m and crown width: 11.25 m) were used with the distance from 15 m (OR $= 0$) to 3.75 m (OR $= 0.75$) and a step of 1.875 m (OR $= 0.125$).

To investigate the effects of point density, we thinned the point cloud of different tree species using the method [58] to NPD $=$ 0.01, 0.02, 0.04, 0.06, 0.08, and 0.1 m. Using the point cloud with varying NPDs, we changed the values of neighbor radius in DBSCAN from 0.15 to 1 m with a step of 0.06 m, and *Dt* values

in the initial segmentation part from 0 to 1.5 m with a step of 0.1 m to explore their effects on segmentation.

IV. Results

We applied the proposed algorithm on the nine plots (Evo-LC1, Evo-LC2, Evo-LC3, Evo-HC4, Evo-HC5, and Evo-HC6) at Evo, and three plots (WPA-LB1, WPA-LM2, and WPA-HB3) at WPA. Detailed information about plots was in Table I. For tree trunk identification, we recorded the H_0 values for stratification surfaces and the tree trunks number correctly identified and incorrectly identified, respectively. For forest 3-D crown segmentation, we recorded TP, FP, and FN value, and calculated the value of *r*, *p*, F1-score for analysis and comparison.

A. Result of Tree Trunk Identification

By applying our proposed the trunk identification step, we obtained the ground, stratification surfaces, tree trunks for the forest plots Evo-LC1 [Fig. 4(a)], Evo-LC2 [Fig. 4(b)], Evo-LC3 [Fig. 4(c)], Evo-HC4 [Fig. 4(d)], Evo-HC5 [Fig. 4(e)], Evo-HC6 [Fig. 4(f)], WPA-LB1 [Fig. 4(g)], WPA-LM2 [Fig. 4(h)], and WPA-HB3 [Fig. 4(i)]. We obtained the ground by filling the missing areas generated by the occlusion of vegetation (Fig. 4). The H_0 for dividing the nine forest plots into overstory and understory layers were 7.78, 5.88, 5.07, 4.86, 5, 2.52, 2.33, 6.48, and 0 m, respectively. The height threshold at plot Evo-LC1 was the largest, and that at plot WPA-HB3 was 0 m because of no understory at this plot. It was found H_0 at low-density forest plots was higher than those at high-density forest plots. Trunks could be extracted from the point cloud accurately (Fig. 4), and obvious differences in trunks extraction were found at each plot. The number of those mistakenly extracted as trunks from point cloud at nine plots was 0, 1, 3, 12, 11, 29, 0, 2, and 4, respectively. Compared to those of low-density plots and high-density plots, it was found that more points were misidentified as trunks at high-density plots than low-density plots. Compared with the Evo forest and WPA forest, it was found that trunk points extracted from Evo were more comprehensive than the WPA forest.

B. Result of Forest 3-D Crown Segmentation

By applying our proposed forest 3-D segmentation algorithm, we obtained the trees segmentation results for overstory and understory, and DTM for forest plots Evo-LC1 [Fig. 5(a)], Evo-LC2 [Fig. 5(b)], Evo-LC3 [Fig. 5(c)], Evo-HC4 [Fig. 5(d)], Evo-HC5 [Fig. 5(e)], Evo-HC6 [Fig. 5(f)], WPA-LB1 [Fig. 5(g)], WPA-LM2 [Fig. 5(h)], and WPA-HB3 [Fig. 5(i)]. Statistics information of the overstory segmentation results was in Table III. At Evo forest plots, *r*, *p*, and F1-score ranged from 0.91 to 1, 0.81 to 1, and 0.85 to 1, respectively. By adding up TP, FN, and FP values in the low-density plots and high-density plots, it was found that *r*, *p*, and F1-score at high-density forest plots were lower than those at low-density forest plots with *r* decreased by 0.04, *p* decreased by 0.11, and F1-score decreased by 0.07. At WPA forest plots, *r*, *p*, F1-score decreased with the number of trees from 0.83 to 0.59, from 1 to 0.71, and from 0.91 to 0.65, respectively. The poorest segmentation result was at WPA-HB3. We calculated the average bias [49], RMSE, and the median value between tree height estimated and true overstory height. The average bias between tree height and estimated in Evo forest ranged from -2.88 to -1.36 m. It means the overstory height obtained was underestimated. Detailed average bias, RMSE, and median information for overstory height were in Table IV. As for the understory, statistics information of understory was in Table III. For all the plots, plot Evo-HC5 had the most understory extracted with 23, and no understory was extracted from plot WPA-HB3. At Evo forest plots, *r*, *p*, and F1-score for understory ranged from 0.65 to 0.84, 0.8 to 1, and 0.73 to 0.86, respectively. Plot Evo-HC6 had the maximum F1-score of 0.86, and plot Evo-LC3 had the minimum F1-score of 0.73. At WPA forest plots, *r*, *p*, F1-score at plot WPA-LB1 were 0.71, 1, and 0.83, respectively. *r*, p, F1-score at WPA-LM2 were 0.67, 0.8, and 0.73, respectively. Compared with true understory height, the average bias between true height and the estimated ranged from -1.67 to 1.56 m. Detailed average bias, RMSE, and median information for understory height were in Table IV. The result showed that understory height was overestimated in Evo forest plots, but it was underestimated in the WPA forest.

V. Discussion

A. Effect of Input Parameters

1) Effect of MDT Value: The MDT had effects on the number of seed points identified in our stratification-based method. Pronounced differences were found for the number of the seed points identified (NSPI) with and without the understory layer (Fig. 6). For plot Evo-LC3 [Fig. 6(c)], as MDT increased from 0 to 0.006 m under the two conditions, NSPI both increased rapidly but less than the true value of 43. This could be attributed to the lower MDT value. Most trunks were filtered because of their more considerable distances between trunk points and cylinder model fitted. Only tree trunks with perfect cylinders remained, for example, the trees inside of the black ellipse in Fig. 5(i). The trunk consisted of discontinuous points was misidentified as the neighbor tree crown rather than the seed point. As MDT increased from 0.006 to 0.017 m, NSPI under two conditions was relatively stable at around 43. As MDT increased from 0.017 to 0.03 m, NSPI under the condition of understory increased from 46 up to 71. The larger MDT value might result in the rapid increase of NSPI. It further caused the understory and partial tree crown points, whose distances to the fitted cylinder model were less than MDT, identified as trunk points. NSPI-based stratification surface was relatively stable at around 43 between 0.006 and 0.03 m, which means MDT value had few effects on the number of seed points identified. Overall, similar variation processes were found at other plots in Fig. 6. It is recommended to use our method to identify seed points and trunk points identification before tree segmentation and avoid the effect of the understory.

2) Effect of R_2 *Value:* R_2 had apparent effects on trunk point identification. It was found that the variation process had three distinct changing stages, such as the rapidly decreasing phase, relatively stable phase, and rapidly increasing phase [Fig. 7(a)]. For the coniferous tree, the error rate rapidly decreased as R_2

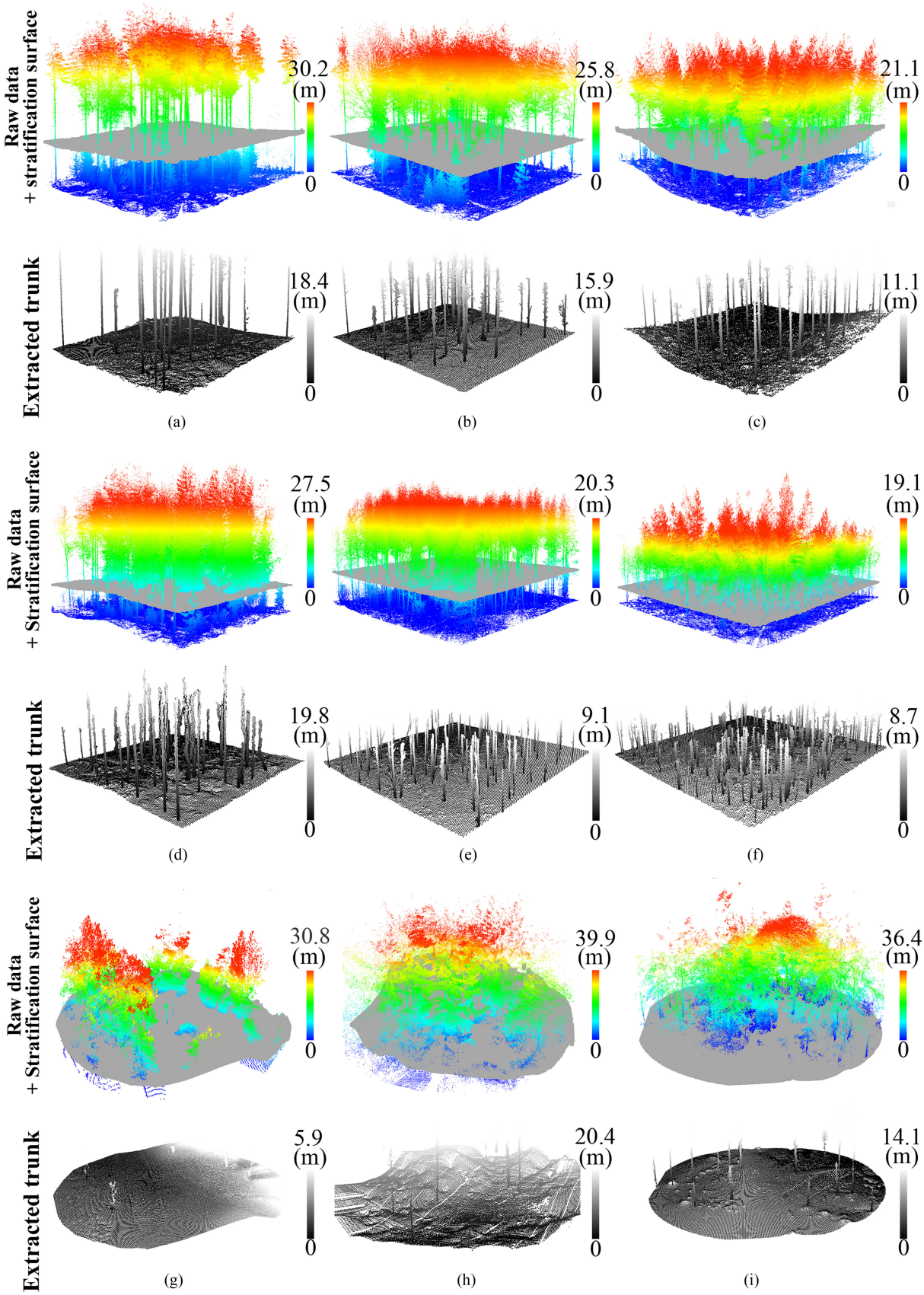

Fig. 4. Ground, stratification surfaces, and trunks obtained at each plot. Fig. 4(a)–(c) are the results of low-density coniferous plots in Evo. Fig. 4(d)–(f) are the results of high-density coniferous plots in Evo. Fig. 4(g) is the result of the low-density broadleaf plot at WPA. Fig. 4(h) is the result of low-density mixed-species plot at WPA. Fig. 4(i) is the result of the high-density broadleaf plot at WPA.

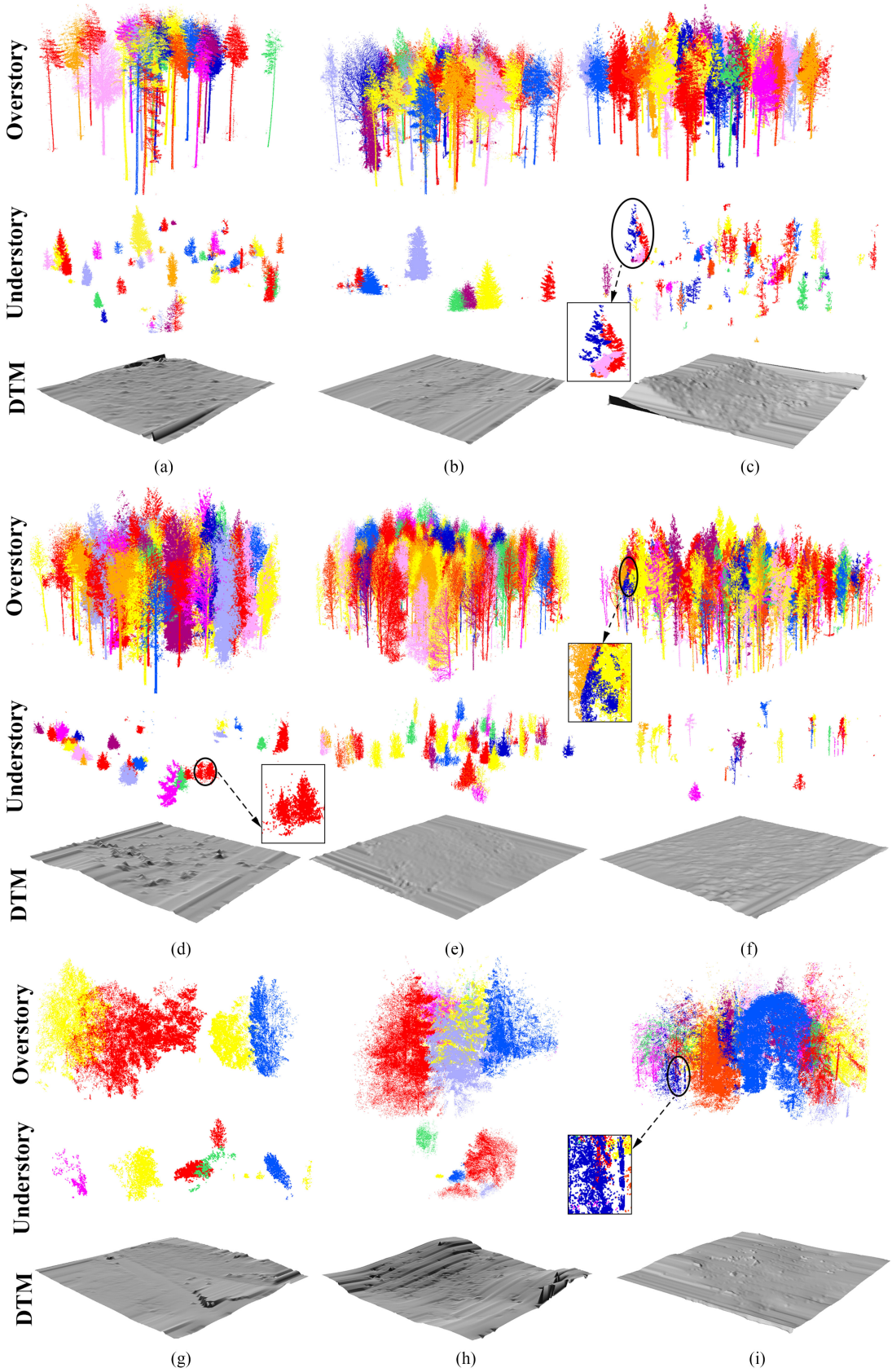

Fig. 5. Overstory and understory segmentation results and DTM generated at each plot. In the segmentation results of overstory and understory, different colors represent different trees extracted. The points inside of the black ellipse were the mis-segmented parts. Fig. 5a-Fig. 5c are the results of low-density coniferous plots in Evo. Fig. 5d-Fig. 5f are the results of high-density coniferous plots in Evo. Fig. 5g is the result of a low-density broadleaf plot at WPA. Fig. 5h is the result of a low-density mixed-species plot at WPA. Fig. 5i is the result of a high-density broadleaf plot at WPA without an existing understory.

TABLE III
OVERSTORY AND UNDERSTORY SEGMENTATION RESULTS OBTAINED FROM THE PROPOSED AND EXISTING ALGORITHM

Overstory segmentation results								
Plot	NT	NST	TP	FP	FN	r	p	F1-score
Evo-LC1(Yun)	27	27	27	0	0	1.00	1.00	1.00
Evo-LC1(Dijkstra-based)	27	27	27	0	0	1.00	1.00	1.00
Evo-LC2(Yun)	36	37	36	1	0	1.00	0.97	0.99
Evo-LC2(Dijkstra-based)	36	38	35	3	1	0.97	0.92	0.95
Evo-LC3(Yun)	43	43	40	3	3	0.93	0.93	0.93
Evo-LC3(Dijkstra-based)	43	43	38	5	5	0.88	0.88	0.88
Evo-HC4(Yun)	55	62	50	12	5	0.91	0.81	0.85
Evo-HC4(Dijkstra-based)	55	65	43	22	12	0.78	0.66	0.72
Evo-HC5(Yun)	92	95	86	9	6	0.93	0.91	0.92
Evo-HC5(Dijkstra-based)	92	96	80	16	12	0.87	0.83	0.85
Evo-HC6(Yun)	145	160	135	25	10	0.93	0.84	0.89
Evo-HC6(Dijkstra-based)	145	115	98	17	47	0.68	0.85	0.75
WPA-LB1(Yun)	6	5	5	0	1	0.83	1.00	0.91
WPA-LB1(Dijkstra-based)	6	5	5	0	1	0.83	1.00	0.91
WPA-LM2(Yun)	8	8	6	2	2	0.75	0.75	0.75
WPA-LM2(Dijkstra-based)	8	10	6	4	2	0.75	0.60	0.67
WPA-HB3(Yun)	17	14	10	4	7	0.59	0.71	0.65
WPA-HB3(Dijkstra-based)	17	13	8	5	9	0.47	0.62	0.53
Understory segmentation results								
Plot	NU	NSU	TP	FP	FN	r	p	F1-score
Evo-LC1	19	20	16	4	3	0.84	0.8	0.82
Evo-LC2	9	7	7	0	2	0.78	1.00	0.88
Evo-LC3	23	18	15	3	8	0.65	0.83	0.73
Evo-HC4	20	20	16	4	4	0.80	0.80	0.80
Evo-HC5	32	23	21	2	11	0.66	0.91	0.76
Evo-HC6	18	17	15	2	3	0.83	0.88	0.86
WPA-LB1	7	5	5	0	2	0.71	1.00	0.83
WPA-LM2	6	6	4	1	2	0.67	0.8	0.73

NT means the number of trees; NST means the number of segmented trees; NU means the number of understory; NSU means the number of segmented understory; TP is the number of correctly extracted tree locations; FN is the number of falsely extracted tree locations; FP is the number of falsely extracted nonexisting tree locations; *r* represents the completeness of crown segmentation; *p* describes the correctness of crown segmentation; F1-score is the overall accuracy considering both commission and omission.

TABLE IV
COMPARISON BETWEEN TREE HEIGHT AND ESTIMATED BASED ON EVO AND WPA DATA

Plot	O_Average (m)	O_RMSE (m)	O_Median (m)	U_Average (m)	U_ RMSE(m)	U_Median(m)
Evo-LC1	-1.43	1.49	-1.41	0.93	0.98	0.89
Evo-LC2	-1.36	2.00	-0.65	1.09	0.54	1.08
Evo-LC3	-1.67	2.61	-0.91	0.97	0.79	0.99
Evo-HC4	-1.88	2.14	-1.52	1.20	1.05	0.73
Evo-HC5	-1.55	1.86	-1.88	1.56	2.49	0.87
Evo-HC6	-1.65	1.87	-1.39	1.41	0.75	1.27
WPA-LB1	-2.31	1.46	-1.67	-1.67	0.75	-1.84
WPA-LM2	-2.33	2.00	-2.00	-1.15	0.35	-1.18
WPA-HB3	-2.88	2.10	-2.40	*None*	*None*	*None*

O_Average, O_RMSE, and O_Median means average bias, RMSE, and the median value for overstory height and estimated. U_Average, U_ RMSE, and U_Median means average bias, RMSE, and the median value for understory height and estimated. *None* means no value was here because of no understory at plot WPA-HB3.

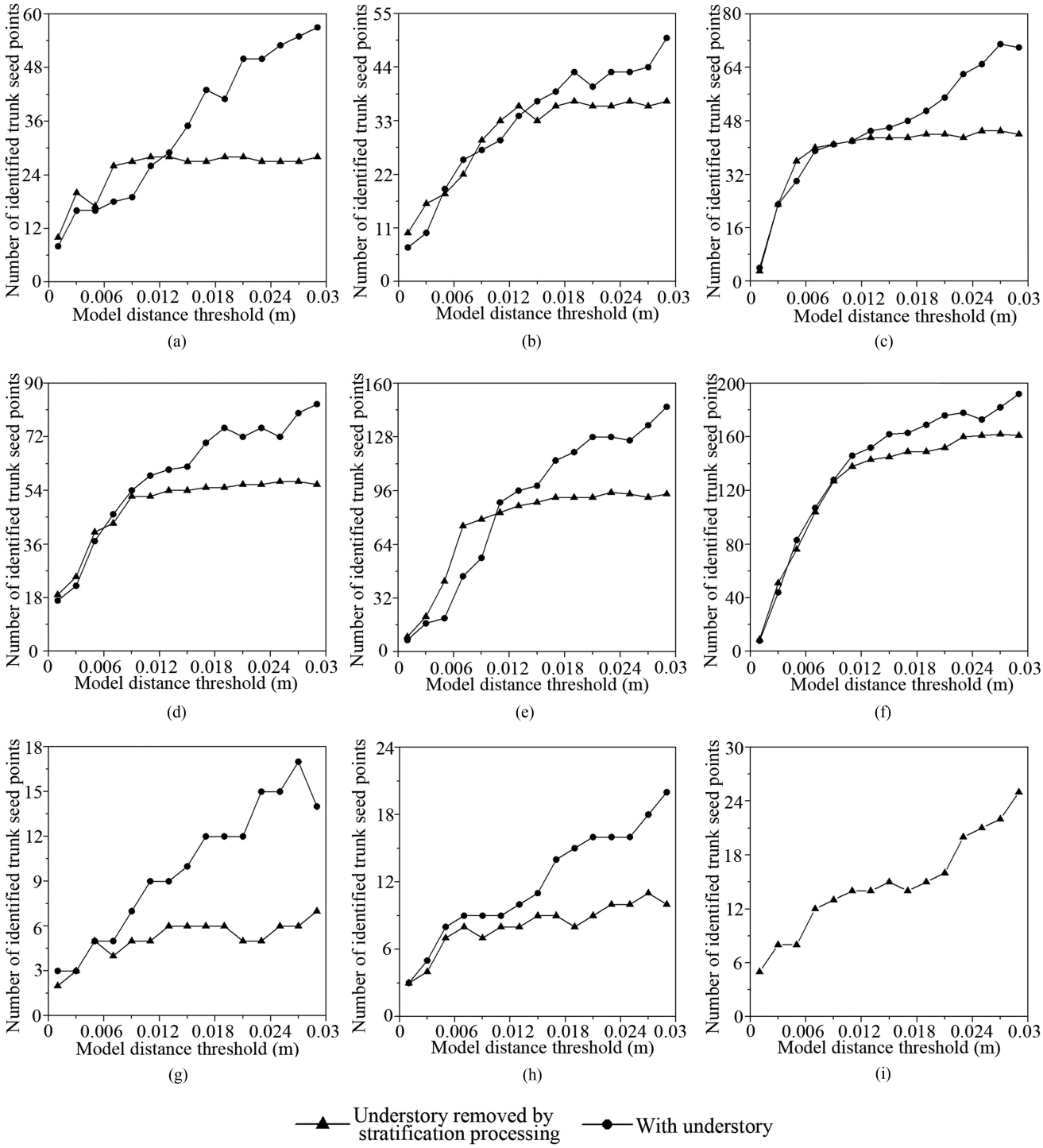

Fig. 6. Effect of model distance threshold (MDT) on seed points identification under the condition of understory removed by our stratification processing. The condition of the slice with understory was not removed. (a)–(c) are the results at low-density plots in Evo. (d)–(f) are the results at high-density plots in Evo. (g) is the result at a low-density plot at WPA. (h) is the result at a low-density plot at WPA. There is no understory at plot WPA-HB3 (i).

increased from 0.05 to 0.35 m was relatively stable when R_2 ranged from 0.35 to 1 m, and then gradually increased up to 0.72 when R_2 was beyond 1 m. When $R_2 < 0.35$ m, the diameter obtained each time was always less than the threshold, part points from ground to treetop were included as trunk points incorrectly. When $R_2 > 1$ m, the trunk level obtained decreased, and upper crown points could be collected mistakenly. Three similar phases appeared in terms of the broadleaf tree and a similar reason for this variation process. By analyzing the effects of R_2 on the error points rate, it is recommended that R_2 should be larger than two times the r detected in the RANSAC algorithm to ensure the tree trunk points are included. In addition, some researchers considered the area with the most vertical accumulation of voxels as a tree trunk [23]. However, the area does not represent the

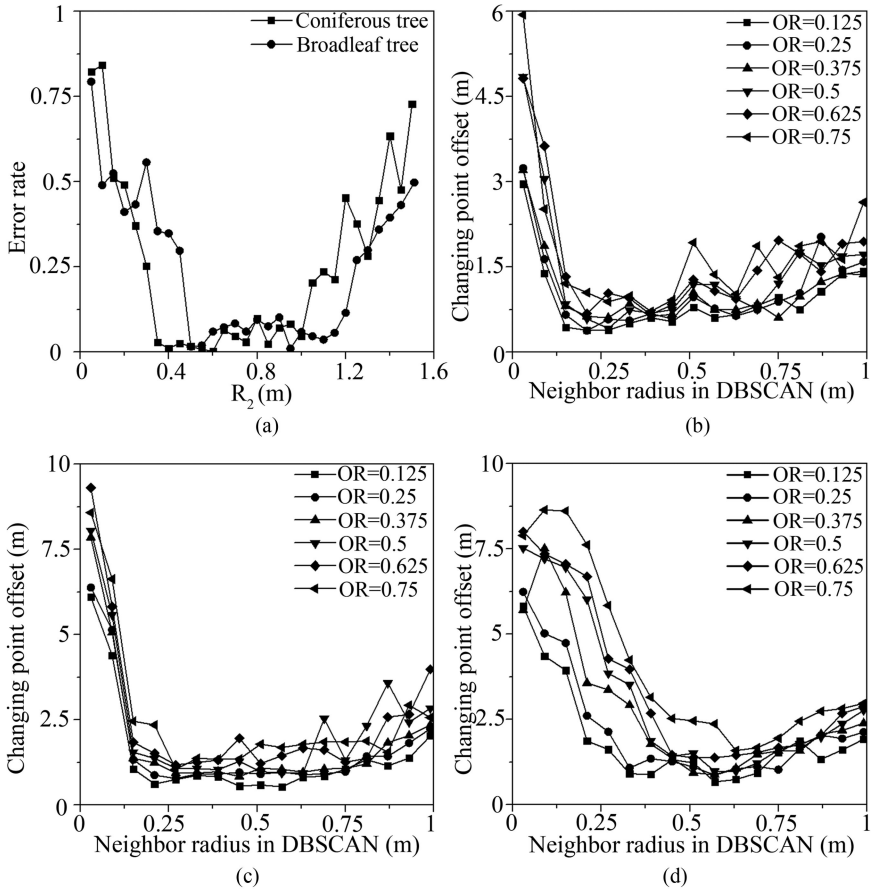

Fig. 7. Effect of R_2 on trunk points identification and effect of neighbor radius in DBSCAN algorithm on changing point at different overlapping rates between trees. R_2 means the radius of the searching sphere in trunk extraction. OR is the overlapping rate between trees. (a) Effect of R_2 on trunk points identification in the coniferous tree. (b) Effect of neighbor radius on changing point in coniferous tree experiment. (c) Effect of neighbor radius on changing point in broadleaf tree experiment. (d) Effect of neighbor radius on changing point in mixed tree species (coniferous and broadleaf trees) experiment.

proper trunk position because the trunk does not grow vertically. Our sphere-searching technique is recommended to ensure the accuracy of curved trunk identification.

3) Effect of Neighbor Radius in DBSCAN Algorithm: The neighbor radius in the DBSCAN algorithm had effects on the accuracy of the changing point detection. For example, comparing the result at a fixed OR in each group, it was found that changing point offset had similar three phases [Fig. 7(b)–(d)]. In coniferous tree experiment, when OR was 0.125, rapidly decreasing, relatively stable, and slowly increasing phases were 0.03–0.15 m, 0.15–0.63 m, and 0.63–0.99 m, respectively. The rapidly decreasing phase could be attributed to the smaller neighbor radius. The smaller radius resulted in the points misallocated to multiple individuals at the layer. Then the changing points were easily detected mistakenly, and the larger changing point offsets were generated. The larger radius caused a slowly increasing phase. A larger neighbor radius caused those points in the layer to cluster several individuals as one individual mistakenly. As the tree shape changed vertically, the algorithm would find other points as the changing points. The changing point offset would lead to the deviation of the determined segmentation plane, and finally, the points were misallocated. Similar variation processes were found in the experiments of broadleaf and mixed tree species (coniferous + broadleaf). However, more segmentation errors would generate when more changing points were detected, for example, the trees in Fig. 5(f). The larger errors were generated from the determination of multiple changing points and then the points allocated mistakenly.

Moreover, we identified the changing points manually from the point cloud, which increased the changing point offset obtained. Overall, the segmentation result was affected by DBSCAN clustering. It is recommended that the neighbor radius should be smaller to obtain a lower changing point offset, but it should be larger than five times the NPD.

B. Effect of Overlapping Rate Between Trees

The OR had apparent effects on the tree segmentation in the 3-D forest stand. For example, apparent differences were found for the segmentation accuracy at Evo and WPA forest plots with varying ORs, and segmentation accuracy decreased as ORs. For the coniferous experiment, the error point number and error rate increased from 0 to 18 547, and 0 to 0.35 as OR increased from 0 to 0.75, respectively (Table V). OR should be less than 0.625 to achieve better crown segmentation accuracy above 0.75 in the coniferous trees. A similar variation process was observed in the

TABLE V
POINTS NUMBER INFORMATION OF OVERLAPPING SEGMENTATION EXPERIMENTS AT DIFFERENT GROUPS

	Distance (m)	OR	Error points number	Error rate
Coniferous (total points: 53538)	5	0	0	0
	4.375	0.125	151	0.01
	3.75	0.250	6,039	0.11
	3.125	0.375	4,894	0.09
	2.5	0.500	9,910	0.19
	1.875	0.625	13,518	0.25
	1.25	0.750	18,547	0.35
Broadleaf (total points: 264325)	20	0	0	0
	17.5	0.125	3,814	0.01
	15	0.250	72,528	0.27
	12.5	0.375	117,580	0.44
	10	0.500	127,949	0.48
	7.5	0.625	136,547	0.52
	5	0.750	168,392	0.64
Coniferous-Broadleaf (Coniferous tree total points: 44575. Broadleaf tree total points: 264325)	15	0	0	0
	13.125	0.125	2,151	0.05
	11.25	0.250	8,867	0.20
	9.375	0.375	15,709	0.35
	7.5	0.500	19,162	0.43
	5.625	0.625	18,146	0.41
	3.75	0.750	20,871	0.47

OR means overlapping rate.

broadleaf experiment. The error rate increased from 0 to 0.64 as the OR increased from 0 to 0.75 in the broadleaf experiment. It means more segmentation errors appear, and the broadleaf forest is more difficult to segment than the coniferous forest. The error rate for the experiment using mixed tree species increased from 0 to 0.47 as OR increased from 0 to 0.75. Summarily, the OR affected the crowns segmentation results, and error points number and error rate would increase as OR increased in three experiments. This could be explained by the complex branch structure in the forest. The higher OR always means the tree crown intersected heavily with more points from other trees, which caused the larger changing point offset [Fig. 7(b)–(d)], for example, the trees inside of black ellipse in Fig 5(d). Two trees were identified as a single tree due to their high OR (unclear boundary) and small spacing. This was consistent with the result in Section V-A-3. As the OR increased, the detection accuracy of changing points would decrease. Eventually, the points' allocation problem appeared. Moreover, the OR varied with tree species, crown shape and size, and canopy cover [60]. This makes it more difficult to segment the crown with heavy overlapping areas.

C. Effect of Scanning Locations

The scanning locations affected the accuracy of tree crowns segmentation and tree height obtained. We tested our algorithm on single-station data at six plots of Evo forest, apparent differences were found for the trees segmentation results based on the multistation TLS data and single-station TLS data, for example, the difference in H_0. H_0 (7.2, 5.5, 4.71, 3.52, 4.2, and 1.71 m) at single-station data were lower than those at multistation data. It could be explained that fewer object details of understory were captured in single-station data than multistation. The segmentation results of single-station data showed that F1-score at six plots was between 0.67 and 0.8 (Table VI), which was lower than the accuracy of multistation data. This could be attributed to the incomplete scanning, which led to the lower detection accuracy of seed points at the plot edge and the changing point leaning in the wrong direction. For segmentation results of single-station data, our accuracy (F1-score was between 0.67 and 0.8 within 15–20 m distance to a scanner) was similar to the result of Liang [31] (F1-score was 0.73 within 10 m distance) and Kenneth [48] (F1-score was 0.87 within 10 m distance). However, Kenneth had confirmed that the segmentation accuracy decreased as the distance to the scanner increased. That was the reason that the trees at the edge of the plot could not be extracted accurately. As for tree height, our result of tree height estimation was consistent with Brolly's [3] result with a mean bias of -2.76 m from single-station and -1.59 m from multistation. Their mean bias in the two modes was -2.9 and -1.3 m, respectively. It was found that overstory height was consistently underestimated due to the occlusion

TABLE VI
SEGMENTATION RESULTS BASED ON SINGLE-STATION TLS DATA IN EVO FOREST

Overstory segmentation results								
Plot	NT	NST	TP	FN	FP	r	p	F1-score
Evo-LC1	27	23	20	7	3	0.74	0.87	0.8
Evo-LC2	36	24	22	14	2	0.61	0.91	0.73
Evo-LC3	43	31	29	14	2	0.67	0.93	0.78
Evo-HC4	55	40	35	20	5	0.63	0.87	0.73
Evo-HC5	92	54	49	43	5	0.53	0.9	0.67
Evo-HC6	145	106	90	55	16	0.62	0.84	0.71
Understory segmentation results								
Plot	NU	NSU	TP	FN	FP	r	p	F1-score
Evo-LC1	19	19	15	4	4	0.79	0.79	0.79
Evo-LC2	9	10	7	2	3	0.78	0.70	0.74
Evo-LC3	23	16	13	7	3	0.65	0.81	0.72
Evo-HC4	20	13	10	10	3	0.50	0.77	0.61
Evo-HC5	32	19	15	17	4	0.47	0.79	0.59
Evo-HC6	18	14	11	7	3	0.61	0.79	0.69

NT means the number of trees; NST means the number of segmented trees; NU means the number of understory; NSU means the number of the segmented understory. TP is the number of correctly extracted tree locations; FN is the number of falsely extracted tree locations; FP is the number of falsely extracted nonexisting tree locations; *r* represents the completeness of crown segmentation; *p* describes the correctness of crown segmentation; F1-score is the overall accuracy considering both commission and omission.

TABLE VII
COMPARISON BETWEEN TREE HEIGHT AND ESTIMATED BASED ON SINGLE-STATION TLS DATA IN EVO

Plot	O_Average	O_RMSE	O_Median	U_Average	U_RMSE	U_Median
Evo-LC1	-2.29	2.10	-2.10	1.15	1.79	0.71
Evo-LC2	-2.42	1.76	-2.40	1.52	2.62	0.88
Evo-LC3	-2.53	2.72	-1.89	0.94	1.89	0.79
Evo-HC4	-3.77	4.60	-2.86	2.51	1.28	2.31
Evo-HC5	-3.16	1.82	-2.72	1.37	1.55	0.85
Evo-HC6	-2.41	2.62	-1.87	0.91	1.49	0.57

O_Average, O_RMSE, and O_Median means average bias, RMSE, and the median value for overstory height and estimated based on single-station data. U_Average, U_RMSE, and U_Median means average bias, RMSE, and the median value for understory height and estimated based on single-station data.

of the tree crowns and lower vertical connectivity. However, understory height was consistently overestimated due to the mixing of overstory and ground points (Table VII). Tree height estimation errors would increase as tree height and tree number increased [61]. That was why the understory height estimated had higher accuracy than overstory. Overall, it is recommended to collect data based on multistation (for example, more than three scanning locations) for better accuracy of segmentation and structural parameters estimation.

D. Effect of Forest Types

Forest type had apparent effects on the trees segmentation accuracy. For example, apparent differences were found for the trees segmentation of the forest point cloud at Evo forest plots [Fig. 5(a)–(f), Table III) and WPA forest plots [Fig. 5(g)–(i), Table III). The average values of *r*, *p*, F1-score in Evo forest were 0.95, 0.91, and 0.93, compared with the average values of *r*, *p*, F1-score in the WPA forest of 0.72, 0.82, and 0.77. It was found that the segmentation accuracy in the coniferous forest was higher than that in the broadleaf forest. The lower accuracy at the broadleaf forest was caused by the complex and heavy intersection between trees with their long branches, which always represents the high OR than coniferous forest. However, the OR affected the segmentation accuracy, and a higher OR means more point allocation problems as analyzed in Section V-B. Moreover, even at the same OR, broadleaf trees had more points allocation problems and a higher error rate than coniferous trees [Fig. 7(b) and (c)]. For example, in Section V-A-3, it was found that the coniferous trees experiment had the lower changing point offset values (less than 0.8 m) at a relatively stable phase than those two broadleaf trees group (more than 1 m) and mixed-species group (more than 1 m).

E. Effect of Vertical Forest Structure

The vertical structure affected the tree crowns segmentation accuracy due to the existence of understory in the forest.

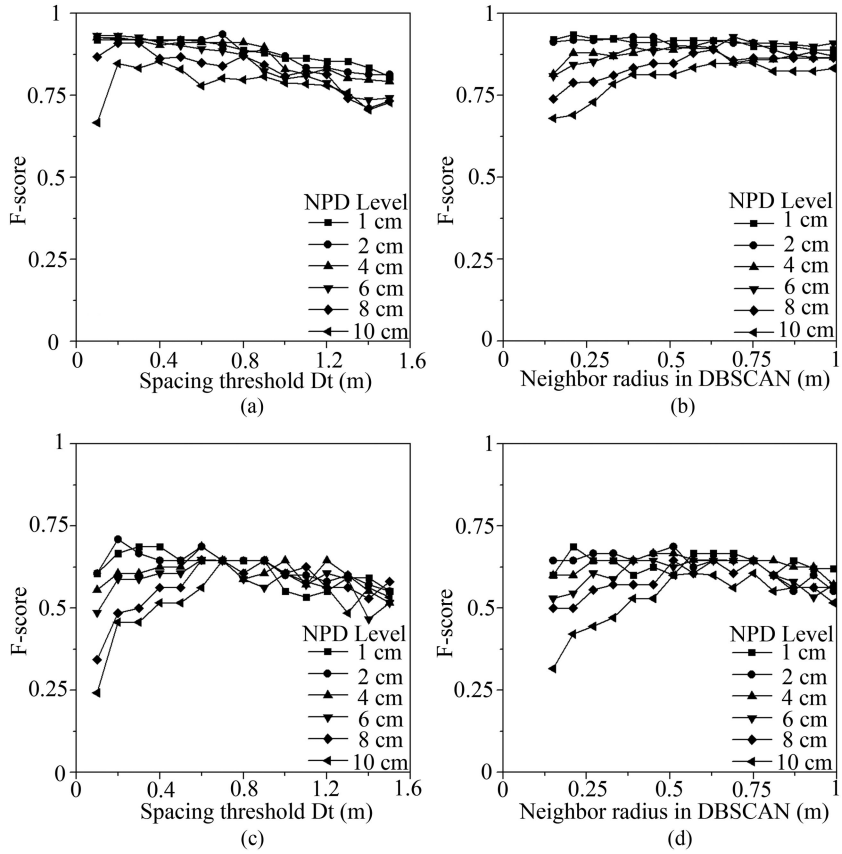

Fig. 8. Effect of point density (NPDs were 1, 2, 4, 6, 8, and 10 cm, respectively), and effect of varying *Dt* and neighbor radius in DBSCAN algorithm under varying NPDs. *Dt* was the spacing threshold used in initial segmentation. NPD was the neighbor point distance of the point cloud. (a) Effect of *Dt* under varying NPDs based on coniferous tree. (b) Effect of neighbor radius in DBSCAN under varying NPDs based on coniferous tree. (c) Effect of *Dt* under varying NPDs based on broadleaf tree. (d) Effect of neighbor radius in DBSCAN under varying NPDs based on broadleaf tree.

Noticeable differences were found for the segmentation results at plots with varying understory (Fig. 5, Table III). In the Evo forest, plots Evo-LC3, Evo-HC4, and Evo-HC5 had more understory (understory number $\geq$ 20) than those (understory number $\leq$ 20) at Evo-LC1, Evo-LC2, and Evo-HC6. For overstory, the average values of *r*, *p*, and F1-score at Evo-LC3, Evo-HC4, and Evo-HC5 were 0.92, 0.88, 0.9, while the average values of *r*, *p*, and F1-score at Evo-LC1, Evo-LC2, and Evo-HC6 were 0.98, 0.94, and 0.96, respectively. The overstory segmentation accuracy at plots with more understory was lower than those plots with less understory. This accuracy difference could be explained by some understory points mixed into the overstory, which decreased the seeds identification accuracy and caused changing point offset. For understory segmentation accuracy, the plots with more understory had lower accuracy. For example, average values of *r*, *p*, and F1-score at the Evo-LC1, Evo-LC2, and Evo-HC6 were 0.82, 0.89, and 0.85, respectively, which were higher than the average value of *r* (0.71), *p* (0.85), and F1-score (0.76) at Evo-LC3, Evo-HC4, and Evo-HC5, respectively. However, it was found that the extracted understory was incomplete, especially the crown of the understory, and those lower shrubs with high OR could not be extracted accurately [missegmented understory inside of the black ellipse in Fig. 5(c)]. This could be attributed to the irregular shape of the understory and the high OR, which led to the difficulty in finding the changing point. To avoid the effect of understory, some researchers removed the understory manually from the point cloud to avoid the effect of understory [60], but it was time-consuming and labor-intensive. It is recommended to stratify the overstory and understory first for better accuracy, and extract them, respectively, in the forest with complex vertical structure.

F. Effect of Point Density

The point density affected the accuracy of tree crowns segmentation. We tested our algorithm at the plot Evo-HC5 and WPA-HB3 with different point densities (NPDs were 1, 2, 4, 6, 8, and 10 cm, respectively). Differences in F1-score were found for the trees segmentation result under varying point densities (Fig. 8). For example, F1-score in high point densities (NPD = 1 cm, 2 cm) was higher than those of low point densities (NPD = 8 cm, and 10 cm). Similar variation processes were found in the coniferous and broadleaf forests. This might be attributed to the different levels of detail recorded in the point cloud with varying point densities. Lower NPD was beneficial to initial segmentation and changing point identification. *Dt* and radius

in DBSCAN were the two key parameters determined according to the value of NPD. The variation process of *Dt* and radius in DBSCAN were in Fig. 8. When *Dt* and radius in DBSCAN were less than 0.3 m, the F1-score increased rapidly. This was because that the lower *Dt* and radius in DBSCAN caused multiple clustering individuals (high FP value). However, the larger *Dt* and radius (for example, NPD $>$ 0.9 m) in DBSCAN would cause under-segmentation. Compared with coniferous forest, under the varying NPD, F1-score in the broadleaf forest had a larger varying range (0.37 and 0.39) than that of coniferous forest (0.21 and 0.24) (Fig. 8). It means the segmentation result of the broadleaf forest is more affected by point density. Overall, the segmentation result was affected by point density. To guarantee the general applicability when the input point cloud data with various point densities, it is recommended that *Dt* and radius in DBSCAN should be larger than 5.5 times of the NPD.

G. Comparison With Existing Methods

To test the performance of the proposed method, we compared the proposed method against the existing methods:

1) Compared with Li's method [28] tested in Tao's study, the F1-score of the proposed method in coniferous forest and broadleaf forest improved 0.2 and 0.05, respectively. This could be attributed to the processing strategy for horizontal overlapping areas and considering the effect of vertical structure in the forest. However, Li's method was mainly used to segment coniferous forest with simple geometry structure in ALS data. The accuracy would decrease when applying TLS data.
2) Compared with the Dijkstra-based method [8] tested in our article, TLS data at the low-density forest (Evo-LC1, Evo-LC2, and Evo-LC3) were segmented correctly by two methods with high accuracy above 0.9. This was because of low complexity and fewer overlapped areas in the low-density forest plots. However, F1-score at high-density forest plots was higher than those using the Dijkstra-based method with an improvement of 0.13, 0.07, and 0.14, respectively. In the WPA site, similar results were found at WPA-LB1, but the F1-score at the plots WPA-LM2 and WPA-LB3 improved 0.08 and 0.12. This may be attributed to the larger errors generated at the comparison process of distance from the point to trunk. However, we proposed a strategy based on the tree's vertical morphology to segment overlapped areas beside the initial segmentation.
3) Compared with Xi's method [35] based on deep learning, the F1-score of the proposed method in coniferous forest improved by 0.15. It is because the method could not extract trees with multiple peaks in tree crowns and overlapped areas. Moreover, the segmentation accuracy was limited by samples size. Thus, the smaller or larger trees could not be detected effectively.

VI. Conclusion

In this article, we proposed a 3-D tree crown delineation method to extract the overstory and understory using TLS data. Our novelty points of the method are as follows. First, we considered the existence of understory into trees segmentation, and decreased the effect of understory on seed points identification. Second, we proposed a method based on multiplane for the segmentation of overlapped tree crowns. Third, we separated and extracted the individual overstory and understory based on the TLS data. And we investigate the effects of OR, the number of TLS scanning stations, forest types, vertical forest structure, and point density on the accuracy of 3-D tree crowns segmentation. Based on our method, we extracted the trees from different forest stands and different TLS measurements. From our results and analysis, we came to the following conclusions:

1) Trees segmentation result was affected by horizontal and vertical structure of the forest. In the coniferous forest, the accuracy based on multistation TLS data at the low-density forest was much higher than that of the high-density forest. The average F1-score at the low-density forest and high-density forest were 0.96 and 0.89, respectively. Compared with coniferous forests, it was more challenging to extract single trees in the broadleaf forest. In the low-density broadleaf forest and low-density mixed forest, F1-score were 0.91and 0.75, respectively. However, in the high-density broadleaf forest, F1-score was 0.65.
2) F1-score based on single-station data in the coniferous forest was between 0.67 and 0.83, which was lower than the accuracy of multistation TLS data. The average segmentation accuracy of 0.78 at low-density plots in single-station data was higher than that of 0.7 at high-density plots.
3) The average overstory F1-score (0.9) at plots with more understory was lower than that (0.96) of the plots with less understory. The average F1-score (0.85) of understory segmentation at plots with less understory was higher than those (0.76) at plots with more understory.

Acknowledgment

This article was conducted at the International Institute for Earth System Science, Nanjing University. The Precision Forestry Cooperative at the University of Washington and the Finnish Geospatial Research Institute provided the lidar data. We appreciate the anonymous reviewers for their valuable suggestions and comments to significantly improve this article.

References

[1] A. Tiemann and I. Ring, "Challenges and opportunities of aligning forest function mapping and the ecosystem service concept in Germany," *Forests*, vol. 9, no. 11, 2018, Art. no. 691.
[2] Q. Yang *et al.*, "The influence of vegetation characteristics on individual tree segmentation methods with airborne lidar data," *Remote Sens.*, vol. 11, no. 23, 2019, Art. no. 2880.
[3] G. Brolly *et al.*, "Voxel-based automatic tree detection and parameter retrieval from terrestrial laser scans for plot-wise forest inventory," *Remote Sens.*, vol. 13, no. 4, 2021, Art. no. 542.
[4] A. Ahmad *et al.*, "Automatic detection and parameter estimation of trees for forest inventory applications using 3D terrestrial lidar," *Remote Sens.*, vol. 9, no. 9, 2017, Art. no. 946.
[5] C. A. Silva *et al.*, "Estimating stand height and tree density in pinus taeda plantations using in-situ data, airborne lidar and k-nearest neighbor imputation," *Anais Da Academia Brasileira De Ciencias*, vol. 90, no. 1, 2018, Art. no. 295.

[6] J. Wu, W. Yao, S. Choi, T. Park, and R. B. Myneni, "A comparative study of predicting DBH and stem volume of individual trees in a temperate forest using airborne waveform lidar," *IEEE Geosci. Remote Sens. Lett.*, vol. 12, no. 11, pp. 2267–2271, Nov. 2015.

[7] L. Li and C. Liu, "A new approach for estimating living vegetation volume based on terrestrial point cloud data," *Plos One*, vol. 14, no. 8, pp. 1–22, 2019.

[8] S. Tao *et al.*, "Segmenting tree crowns from terrestrial and mobile lidar data by exploring ecological theories," *ISPRS J. Photogramm. Remote Sens.*, vol. 110, pp. 66–76, 2015.

[9] C. B. Field *et al.*, "Primary production of the biosphere: Integrating terrestrial and oceanic components," *Science*, vol. 281, no. 5374, pp. 237–240, 1998.

[10] K. Ma *et al.*, "A novel vegetation point cloud density tree-segmentation model for overlapping crowns using UAV lidar," *Remote Sens.*, vol. 13, no. 8, 2021, Art. no. 20.

[11] R. Leiterer *et al.*, "Forest canopy-structure characterization: A data-driven approach," *Forest Ecol. Manage.*, vol. 358, pp. 48–61, 2015.

[12] L. Eysn *et al.*, "A benchmark of lidar-based single tree detection methods using heterogeneous forest data from the alpine space," *Forests*, vol. 6, no. 12, pp. 1721–1747, 2015.

[13] J. R. G. Bragra *et al.*, "Tree crown delineation algorithm based on a convolutional neural network," *Remote Sens.*, vol. 12, no. 1288, pp. 1–27, 2020.

[14] B. Wu *et al.*, "Individual tree crown delineation using localized contour tree method and airborne lidar data in coniferous forests," *Int. J. Appl. Earth Observ. Geoinf.*, vol. 52, pp. 82–94, 2016.

[15] T. Yun *et al.*, "Individual tree crown segmentation from airborne lidar data using a novel Gaussian filter and energy function minimization-based approach," *Remote Sens. Environ.*, vol. 256, Apr. 2021, Art. no. 112307.

[16] A. H. Ozcan *et al.*, "Tree crown detection and delineation in satellite images using probabilistic voting," *Remote Sens. Lett.*, vol. 8, no. 8, pp. 761–770, 2017.

[17] Z. Zhen, L. J. Quackenbush, and L. Zhang, "Impact of tree-oriented growth order in marker-controlled region growing for individual tree crown delineation using airborne laser scanner (ALS) data," *Remote Sens.*, vol. 6, no. 1, pp. 555–579, 2014.

[18] L. Ene, E. Naesset, and T. Gobakken, "Single tree detection in heterogeneous boreal forests using airborne laser scanning and area-based stem number estimates," *Int. J. Remote Sens.*, vol. 33, no. 16, pp. 5171–5193, 2012.

[19] B. Koch, U. Heyder, and H. Weinacker, "Detection of individual tree crowns in airborne lidar data," *Photogramm. Eng. Remote Sens.*, vol. 72, no. 4, pp. 357–363, 2006.

[20] R. Khorrami *et al.*, "A new method for detecting individual trees in aerial lidar point clouds using absolute height maxima," *Environ. Monit. Assessment*, vol. 190, no. 12, 2018, Art. no. 708.

[21] C. Vega *et al.*, "PTrees: A point-based approach to forest tree extraction from lidar data," *Int. J. Appl. Earth Observ. Geoinf.*, vol. 33, no. 1, pp. 98–108, 2014.

[22] C. Toth and G. Jóźków, "Remote sensing platforms and sensors: A survey," *ISPRS J. Photogramm. Remote Sens.*, vol. 115, pp. 22–36, 2016.

[23] L. Zhong, L. Cheng, H. Xu, Y. Wu, Y. Chen, and M. Li, "Segmentation of individual trees from TLS and MLS data," *IEEE J. Sel. Topics Appl. Earth Observ. Remote Sens.*, vol. 10, no. 2, pp. 774–787, Feb. 2017.

[24] V. F. Strîmbu and B. M. Strîmbu, "A graph-based segmentation algorithm for tree crown extraction using airborne lidar data," *ISPRS J. Photogramm. Remote Sens.*, vol. 104, pp. 30–43, 2015.

[25] C. Paris, D. Kelbe, J. van Aardt, and L. Bruzzone, "A novel automatic method for the fusion of ALS and TLS lidar data for robust assessment of tree crown structure," *IEEE Trans. Geosci. Remote Sens.*, vol. 55, no. 7, pp. 3679–3693, Jul. 2017.

[26] M. Holopainen *et al.*, "Tree mapping using airborne, terrestrial and mobile laser scanning—A case study in a heterogeneous urban forest," *Urban Forestry Urban Greening*, vol. 12, no. 4, pp. 546–553, 2013.

[27] S. Srinivasan *et al.*, "Terrestrial laser scanning as an effective tool to retrieve tree level height, crown width, and stem diameter," *Remote Sens.*, vol. 7, no. 2, pp. 1877–1896, 2015.

[28] W. Li, Q. Guo, M. K. Jakubowski, and M. Kelly, "A new method for segmenting individual trees from the lidar point cloud," *Photogramm. Eng. Remote Sens.*, vol. 78, no. 1, pp. 75–84, 2012.

[29] D. Zhao, Y. Pang, Z. Li, and L. Liu, "Isolating individual trees in a closed coniferous forest using small footprint lidar data," *Int. J. Remote Sens.*, vol. 35, no. 20, pp. 7199–7218, 2014.

[30] W. Yao, P. Krzystek, and M. Heurich, "Tree species classification and estimation of stem volume and DBH based on single tree extraction by exploiting airborne full-waveform lidar data," *Remote Sens. Environ.*, vol. 123, pp. 368–380, 2012.

[31] X. Liang, P. Litkey, J. Hyyppa, H. Kaartinen, M. Vastaranta, and M. Holopainen, "Automatic stem mapping using single-scan terrestrial laser scanning," *IEEE Trans. Geosci. Remote Sens.*, vol. 50, no. 2, pp. 661–670, Feb. 2012.

[32] T. Mizoguchi and Y. Kobayashi, "Interactive trunk extraction from forest point cloud," *Int. Arch. Photogramm. Remote Sens. Spatial Inf. Sci.*, vol. XL, no. 65, pp. 433–436, Jun. 2014.

[33] M. Chen, Y. Wan, M. Wang, and J. Xu, "Automatic stem detection in terrestrial laser scanning data with distance-adaptive search radius," *IEEE Trans. Geosci. Remote Sens.*, vol. 56, no. 5, pp. 2968–2979, May 2018.

[34] S. Xia *et al.*, "Detecting stems in dense and homogeneous forest using single-scan TLS," *Forests*, vol. 6, no. 11, pp. 3923–3945, 2015.

[35] Z. Xi and C. Hopkinson, "Detecting individual-tree crown regions from terrestrial laser scans with an anchor-free deep learning model," *Can. J. Remote Sens.*, vol. 47, no. 2, pp. 228–242, 2020.

[36] H. Luo *et al.*, "Individual tree extraction from urban mobile laser scanning point clouds using deep pointwise direction embedding," *ISPRS J. Photogramm. Remote Sens.*, vol. 175, pp. 326–339, 2021.

[37] Y. Chen *et al.*, "Rapid urban roadside tree inventory using a mobile laser scanning system," *IEEE J. Sel. Topics Appl. Earth Observ. Remote Sens.*, vol. 12, no. 9, pp. 3690–3700, Sep. 2019.

[38] E. W. Dijkstra, "A note on two problems in connecion with graphs," *Numerische Math.*, vol. 1, pp. 269–271, 1959.

[39] C. Cabo, C. Ordóñez, C. A. López-Sánchez, and J. Armesto, "Automatic dendrometry: Tree detection, tree height and diameter estimation using terrestrial laser scanning," *Int. J. Appl. Earth Observ. Geoinf.*, vol. 69, pp. 164–174, 2018.

[40] R. Klein, *Concrete and Abstract Voronoi Diagrams*. Berlin Germany: Springer, 1989.

[41] Y. Liu, R. Liu, J. Pisek, and J. Chen, "Separating overstory and understory leaf area indices for global needleleaf and deciduous broadleaf forests by fusion of MODIS and MISR data," *Biogeosciences*, vol. 14, no. 5, pp. 1093–1110, Mar. 2017.

[42] H. Hamraz, M. A. Contreras, and J. Zhang, "Vertical stratification of forest canopy for segmentation of understory trees within small-footprint airborne lidar point clouds," *ISPRS J. Photogramm. Remote Sens.*, vol. 130, pp. 385–392, 2017.

[43] A. Ferraz *et al.*, "3-D mapping of a multi-layered mediterranean forest using ALS data," *Remote Sens. Environ.*, vol. 121, pp. 210–223, 2012.

[44] D. Kim, R. Oren, and S. S. Qian, "Response to CO_2 enrichment of understory vegetation in the shade of forests," *Global Change Biol.*, vol. 22, no. 2, pp. 944–956, 2016.

[45] J. S. Rentch, M. A. Fajvan, and R. R. Hicks, "Oak establishment and canopy accession strategies in five old-growth stands in the central hardwood forest region," *Forest Ecol. Manage.*, vol. 184, no. 1–3, pp. 285–297, 2003.

[46] J. G. Vogel and S. T. Gower, "Carbon and nitrogen dynamics of boreal jack pine stands with and without a green alder understory," *Ecosystems*, vol. 1, no. 4, pp. 386–400, 1998.

[47] B. Koch, U. Heyder, and H. Weinacker, "Detection of individual tree crowns in airborne lidar data," *Photogramm. Eng. Remote Sens.*, vol. 72, no. 4, pp. 357–363, 2006.

[48] O. Kenneth, H. Johan, and O. HåKan, "Tree stem and height measurements using terrestrial laser scanning and the RANSAC algorithm," *Remote Sens.*, vol. 6, no. 5, pp. 4323–4344, 2014.

[49] J. Hyyppa, O. Kelle, M. Lehikoinen, and M. Inkinen, "A segmentation-based method to retrieve stem volume estimates from 3-D tree height models produced by laser scanners," *IEEE Trans. Geosci. Remote Sens.*, vol. 39, no. 5, pp. 969–975, May 2001.

[50] S. C. Popescu, R. H. Wynne, and R. F. Nelson, "Measuring individual tree crown diameter with lidar and assessing its influence on estimating forest volume and biomass," *Can. J. Remote Sens.*, vol. 29, no. 5, pp. 564–577, 2003.

[51] S. Tao *et al.*, "Airborne lidar-derived volume metrics for aboveground biomass estimation: A comparative assessment for conifer stands," *Agricultural Forest Meteorol.*, vol. 198, pp. 24–32, Nov./Dec. 2014.

[52] X. Liang *et al.*, "International benchmarking of terrestrial laser scanning approaches for forest inventories," *ISPRS J. Photogramm. Remote Sens.*, vol. 144, pp. 137–179, 2018.

[53] W. Zhang *et al.*, "An easy-to-use airborne lidar data filtering method based on cloth simulation," *Remote Sens.*, vol. 8, no. 6, 2016, Art. no. 501.
[54] M. Mcdaniel *et al.*, "Terrain classification and identification of tree stems using ground-based lidar," *J. Field Robot.*, vol. 29, no. 6, pp. 891–910, 2012.
[55] L. I. Duncanson, B. D. Cook, G. C. Hurtt, and R. O. Dubayah, "An efficient, multi-layered crown delineation algorithm for mapping individual tree structure across multiple ecosystems," *Remote Sens. Environ.*, vol. 154, pp. 378–386, Nov. 2014.
[56] D. Jaskierniak *et al.*, "Extracting lidar indices to characterize multilayered forest structure using mixture distribution functions," *Remote Sens. Environ.*, vol. 115, no. 2, pp. 573–585, 2011.
[57] R. C. Bolles and M. A. Fischler, "A RANSAC-based approach to model fitting and its application to finding cylinders in range data," in *Proc. Int. Joint Conf. Artif. Intell.*, 1981, pp. 637–643.
[58] L. Ma *et al.*, "Retrieving forest canopy extinction coefficient from terrestrial and airborne lidar," *Agricultural Forest Meteorol.*, vol. 236, pp. 1–21, 2017.
[59] M. Ester, "A density-based algorithm for discovering clusters in large spatial databases with noise," in *Proc. Int. Conf. Knowl. Discovery Data Mining*, 1996, pp. 226–231.
[60] X. Wang *et al.*, "Characterizing the spatial variations of forest sunlit and shaded components using discrete aerial lidar," *Remote Sens.*, vol. 12, no. 7, 2020, Art. no. 1071.
[61] D. Zande *et al.*, "Influence of measurement set-up of ground-based lidar for derivation of tree structure," *Agricultural Forest Meteorol.*, vol. 141, pp. 147–160, 2006.

Zengxin Yun received the M.Sc. degree in geographic and oceanographic sciences from Nanjing University, Nanjing China, in 2019. He is currently working toward the Ph.D. degree in stratifying the forest overstory and understory for 3-D segmentation using the ALS and TLS data, respectively, with Nanjing University, Nanjing, China.

His research interests include application of light detection and raging in retrieving forest canopy structural parameters and forest ecosystems.

Guang Zheng received the Ph.D. degree in forest resources management from the University of Washington, Seattle, WA, USA, in 2011.

He is currently an Associate Professor of remote sensing with the International Institute for Earth System Science, Nanjing University, Nanjing, China. His research interests include applications of multisource remotely sensed data, particularly light detection and ranging technology in retrieving forest structural parameters at multiple spatial scales and forest aboveground biomass mapping and update using a process-based ecological model.